Cell Biology:

An Autoinhibited Structure of α-Catenin and Its Implications for Vinculin Recruitment to Adherens Junctions

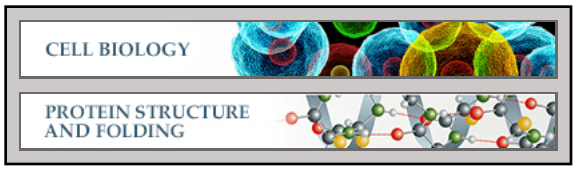

Noboru Ishiyama, Nobutoshi Tanaka, Kentaro Abe, Yoo Jeong Yang, Yazan M. Abbas, Masataka Umitsu, Bhushan Nagar, Stephanie A. Bueler, John L. Rubinstein, Masatoshi Takeichi and Mitsuhiko Ikura

J. Biol. Chem. 2013, 288:15913-15925.
doi: 10.1074/jbc.M113.453928 originally published online April 15, 2013

THE JOURNAL OF BIOLOGICAL CHEMISTRY VOL. 288, NO. 22, pp. 15913–15925, May 31, 2013

An Autoinhibited Structure of α-Catenin and Its Implications for Vinculin Recruitment to Adherens Junctions*[S]

Received for publication, January 16, 2013, and in revised form, March 18, 2013 Published, JBC Papers in Press, April 15, 2013, DOI 10.1074/jbc.M113.453928

Noboru Ishiyama[‡1], Nobutoshi Tanaka[§¶], Kentaro Abe[§], Yoo Jeong Yang[‡], Yazan M. Abbas[‖], Masataka Umitsu[‡], Bhushan Nagar[‖], Stephanie A. Bueler[**], John L. Rubinstein[‡‡§§], Masatoshi Takeichi[¶], and Mitsuhiko Ikura[‡§§2]**

From the [‡]Campbell Family Cancer Research Institute, Ontario Cancer Institute and [§§]Department of Medical Biophysics, University of Toronto, Toronto, Ontario M5G 1L7, Canada, the [§]Graduate School of Biostudies, Kyoto University, Kyoto 606-8501, Japan, the [¶]RIKEN Center for Developmental Biology, Kobe 650-0047, Japan, the [‖]Department of Biochemistry and Groupe de Recherche Axe sur la Structure des Proteines, McGill University, Montreal, Quebec H3G 0B1, Canada, and the [**]Molecular Structure and Function Program, The Hospital for Sick Children Research Institute and [‡‡]Department of Medical Biophysics, University of Toronto, Toronto, Ontario M5G 1L7, Canada

Background: α-Catenin is an actin-binding protein that recruits vinculin to adherens junctions.
Results: An elongated autoinhibited structure of α-catenin indicates structural and functional coupling of its vinculin- and actin-binding mechanisms.
Conclusion: The anchoring strength of adherens junctions is dynamically regulated by α-catenin to match the actomyosin-generated tension.
Significance: Multistate conformations of α-catenin facilitate the direct and vinculin-assisted linkages between the cadherin-catenin complex and the actin cytoskeleton.

α-Catenin is an actin- and vinculin-binding protein that regulates cell-cell adhesion by interacting with cadherin adhesion receptors through β-catenin, but the mechanisms by which it anchors the cadherin-catenin complex to the actin cytoskeleton at adherens junctions remain unclear. Here we determined crystal structures of αE-catenin in the autoinhibited state and the actin-binding domain of αN-catenin. Together with the small-angle x-ray scattering analysis of full-length αN-catenin, we deduced an elongated multidomain assembly of monomeric α-catenin that structurally and functionally couples the vinculin- and actin-binding mechanisms. Cellular and biochemical studies of αE- and αN-catenins show that αE-catenin recruits vinculin to adherens junctions more effectively than αN-catenin, partly because of its higher affinity for actin filaments. We propose a molecular switch mechanism involving multistate conformational changes of α-catenin. This would be driven by actomyosin-generated tension to dynamically regulate the vinculin-assisted linkage between adherens junctions and the actin cytoskeleton.

The cadherin-catenin complex mediates the formation of intercellular adherens junctions (AJs)[3] by having cadherins on adjoining cells participating in the Ca^{2+}-dependent homotypic interactions, whereas connecting intracellularly to the actin cytoskeleton and various signaling pathways through the catenins (1). Coordination of the extracellular and cytoplasmic events by the cadherin-catenin complex is crucial for AJs to be stable enough to support tissue structure and integrity, as well as to remain sufficiently dynamic to rapidly disassemble obsolete connections and foster new junctions during morphogenesis (2–4). The cadherin-catenin complex consists of the cadherin adhesion receptor and the catenins, which include α-catenin, β-catenin, and p120 catenin (supplemental Fig. S1*A*). Although β-catenin and p120 catenin directly bind to the cytoplasmic tail of cadherin and regulate the stability of cadherin on the cell surface (5), α-catenin, an actin-binding protein, indirectly associates with cadherin through β-catenin and anchors AJs to the actin cytoskeleton. Three types of α-catenin have been identified in mammals, designated as αE-catenin, αN-catenin, and αT-catenin (6). Their critical role in cell adhesion is underscored by pathological consequences of deletion or truncation of α-catenin genes in mammals, such as cancer metastasis (7), cerebellar hypoplasia (8), and arrhythmogenic cardiomyopathy (9). As well, the embryonic lethality has been reported for α-catenin-null flies (10). Cell biology studies revealed that αE-catenin is essential for organization of the apical junctional complex (AJC) (11), containing tight junction and AJ, by forming two types of AJs, punctum adherens and zonula adherens, in polarized epithelial cell monolayer (supplemental Fig. S1*B*) (12), and αN-catenin is required for synapse stability in hippocampal neurons (13).

A traditional model of cell-cell adhesion assumed that α-catenin would directly connect the cadherin-catenin com-

* This work was supported in part by grants from the Canadian Cancer Society (to M. I.).
[S] This article contains supplemental Figs. S1–S9.
The atomic coordinates and structure factors (codes 4K1N and 4K1O) have been deposited in the Protein Data Bank (http://wwpdb.org/).
[1] Recipient of a Canadian Institutes of Health Research postdoctoral fellowship.
[2] Holds a Canada Research Chair in Cancer Structural Biology. To whom correspondence should be addressed: Campbell Family Cancer Research Institute, Ontario Cancer Institute and Department of Medical Biophysics, University of Toronto, Toronto, Ontario M5G 1L7, Canada. Tel.: 416-581-7550; Fax: 416-581-7564; E-mail: mikura@uhnres.utoronto.ca.
[3] The abbreviations used are: AJ, adherens junction; AJC, apical junctional complex; SAXS, small-angle x-ray scattering; PDB, Protein Data Bank; DEN, deformable elastic network; VBS, vinculin-binding site; EGFP, enhanced green fluorescent protein; TCEP, Tris(2-carboxyethyl)phosphine.

plex and actin filaments (F-actin), but this model was called into question when previous studies revealed that the interaction between cadherin-catenin complexes and F-actin is much weaker than expected, and that these showed different levels of mobility at AJs (14, 15). Currently, at least four potential actin-binding modes of α-catenin have been proposed (supplemental Fig. S1*C*): autoinhibited state (15), allosteric-binding state involving α-catenin homodimers binding to F-actin near AJs (14), direct-binding state (16), and indirect-binding state through other actin-binding proteins, such as vinculin (17, 18) and EPLIN (epithelial protein lost in neoplasm; also known as Lima-1) (12, 19). Nonetheless, recent studies have shown that monomeric α-catenin bound to the cadherin·β-catenin complex mediates the physical linkage between AJs and the actin cytoskeleton (20), and that cadherin is constitutively under actomyosin-generated tension (21, 22). Moreover, α-catenin has been proposed to act as a mechanosensor in AJ formation by facilitating the recruitment of vinculin to AJs in the actomyosin-derived tension-dependent manner (17). However, how α-catenin regulates the linkage between the cadherin-catenin complex and the actin cytoskeleton by translating the mechanical forces into biochemical signals remains unclear.

α-Catenin has a modulatory architecture that consists of three major domains with distinct functionalities (Fig. 1*A*): an N-terminal (N) domain participates in β-catenin binding and homodimerization (23, 24); a modulatory (M) domain interacts with several actin-binding proteins, including a closely related actin-binding protein vinculin (17, 25, 26); and a C-terminal (C) domain directly (16) and/or indirectly (19, 27) binds to F-actin. As αE- and αN-catenins share 82% primary sequence identity (supplemental Fig. S2), these proteins should be structurally related to each other. Also, α-catenin and vinculin share ~30% sequence identity at three distinct vinculin homology regions, VH1, VH2, and VH3 (Fig. 1*A*), suggesting some commonalities between these proteins as well. It is, however, unclear how three domains of α-catenin are structurally and functionally coupled together in a full-length molecule, as currently available crystallographic details are limited to the individual N- and M-domain fragments of αE-catenin (24, 25, 28–30).

To better understand how α-catenin facilitates actomyosin-dependent tension-induced recruitment of vinculin to AJs, we employed x-ray crystallography, small-angle x-ray scattering (SAXS), and other complementary methodologies to reveal how the assembly of different functional domains within a full-length mouse α-catenin molecule facilitates a unique activation mechanism of α-catenin involving multistate conformational changes.

EXPERIMENTAL PROCEDURES

Protein Expression and Purification—Mouse αE-catenin was cloned into the pET28a vector (Novagen) and expressed as an N-terminal His fusion protein. Mouse αN-catenin, αN-catenin C domain, and human vinculin D1 domain were cloned into the pGEX4T1 vector (GE Healthcare) and expressed as N-terminal glutathione *S*-transferase (GST) fusion proteins. Site-directed mutagenesis was performed using the QuikChange protocol (Stratagene) to produce all single residue and deletion mutants. Recombinant proteins were expressed in *Escherichia coli* BL21-CodonPlus (Stratagene) strain for overnight at 288 K. After collection by centrifugation, cells were resuspended in lysis buffer (50 mM Tris-HCl, pH 8.0, 300 mM NaCl, 10 mM β-mercaptoethanol, 1 mM TCEP), sonicated on ice, and subjected to centrifugation to separate proteins in the soluble fraction. His fusion proteins were isolated using nickel-nitrilotriacetic acid resin (Qiagen). GST fusion proteins were isolated using glutathione-Sepharose resin (GE Healthcare). His and GST fusion proteins were cleaved by thrombin to remove the affinity tags and the cleaved proteins were further purified by size-exclusion chromatography using either Superdex 75 or Superdex 200 (GE Healthcare). The purified proteins were exchanged into protein storage buffer (50 mM Tris-HCl, pH 8.0, 100 mM NaCl, 1 mM TCEP).

Crystallization and Data Collection—Crystals of full-length αE-catenin were obtained by incubating a protein solution containing purified full-length αE-catenin from the monomer fraction (10 mg/ml) against a crystallization solution (0.2 M sodium citrate, 20% (w/v) PEG-3350) by vapor diffusion at 293 K. Crystals were often attached to the crystallization plate or to a skin of denatured protein on the surface on the drop. Dimeric full-length αE-catenin and monomeric full-length αN-catenin samples were also subjected to crystallization, however, these efforts were fruitless. For the crystallization of the α-catenin C domain, a proteolytically stable fragment of the C domain (residues 652–906) was identified when the full-length αE-catenin sample was subjected to degradation under nonreducing conditions during purification. The equivalent region of the αN-catenin C domain (αNcatC; residues 651–905) was cloned, expressed, purified, and crystallized by incubating a protein solution (20 mg/ml) against a crystallization solution (0.1 M HEPES, pH 7.0, 1.6 M $(NH_4)_2SO_4$, 0.2 M NaCl, and 0.1 M K/Na tartate) by vapor diffusion at 277 K. Selenomethione-substituted αNcatC was expressed, purified, and crystallized in the same manner. Crystals were briefly soaked in crystallization solution containing 20% glycerol for data collection at 100 K. Diffraction data were collected at the Advanced Photon Source beamlines 19BM and 19ID (Argonne National Laboratory, Argonne, IL) and processed with HKL2000 (31). Statistics pertaining to the diffraction data are presented in Table 1.

Crystal Structure Determination and Refinement—The crystal structure of αEcatNM was determined at 6.5-Å resolution. The structure solution was solved by molecular replacement with PHASER (32) using the αE-catenin N domain residues 82–262 (PDB code 1DOV) as a search model for the N domain and a homology model of αE-catenin $M_{II\text{-}III}$ regions generated from the full-length vinculin structure (PDB code 1ST6) as a search model for the M domain. For refinement at 6.5-Å resolution, the deformable elastic network (DEN) refinement was performed by using CNS 1.3 (33) as previously described (34), except for the sole implementation of overall anisotropic *B*-factor refinement and the constitutive use of the DEN restraints throughout the process (35). The optimum values of the γ and W_{DEN} parameters of DEN refinement were determined by a two-dimensional grid search using the SBGrid DEN refinement portal. The M_I region in the "unfurled" conformation was modified according to σ_A-weighted difference electron density maps ($2F_o - F_c$ and $F_o - F_c$) and a simulated annealing omit

TABLE 1
Crystallographic data statistics

	αEcatNM	αNcatC (native)	αNcatC (SeMet-substituted)
Data collection			
Space group	$P\,3_2$	$P\,3_212$	$P\,3_212$
Cell dimensions			
a, b, c (Å)	144.7, 144.7, 136.8	112.3, 112,3, 55.9	112.2, 112.2, 56.3
Wavelength (Å)	0.97918	0.97911	0.97915
Resolution range (Å)	50–6.5	50–2.6	50–3.0
$R_{sym}(I)$ (%)	12.8 (52.1)[a]	4.9 (51.9)	15.2 (84.3)
$I/\sigma(I)$	11.6 (3.4)	40.2 (4.1)	12.2 (4.8)
Number of reflections	34,089	111,198	94,278
Unique reflections	6,584	11,888	8,357
Completeness (%)	99.7 (100)	99.7 (100)	99.6 (100)
Redundancy	5.2 (5.5)	9.0 (6.3)	11.1 (11.1)
Refinement			
Resolution range (Å)	50–6.5	40–2.6	
R_{cryst}/R_{free} (%)	22.4/24.8	19.5/23.1	
Model residues	85–262, 290–631	662–861	
Root mean square deviations			
Bond lengths (Å)	0.003	0.008	
Bond angles (°)	0.813	1.104	

[a] Values in parentheses are for the highest resolution shell.

$F_o - F_c$ map of the M_I region by manual model building using Coot (36). The crystal structure of αNcatC was initially determined at 3.0-Å resolution by the single-wavelength anomalous dispersion method, and further refined at 2.6 Å by using PHENIX (37). Refinement statistics are presented in Table 1. Electrostatic surface potential values of the α-catenin and vinculin structures were calculated using APBS (38). Molecular graphics representations were prepared using PyMOL.

Mammalian Expression Plasmid Construction and Transfection—Full-length or deletion clones for αE- and αN-catenin genes were amplified by PCR, and subcloned into pCA-sal-EGFP-IRES-hygro vector (39). To generate chimeric constructs, 1–662 and 663–906 amino acids fragments of αE-catenin were fused with 662–905 and 1–661 amino acids fragments of αN-catenin, respectively, by using overlapping PCR method. R2/7 cells were cultured in a 1:1 mixture of DME and Ham's F-12 medium (Iwaki) supplemented with 10% fetal calf serum (FCS). Cells were transfected with expression vectors by using Effectene Transfection Reagent (Qiagen), according to the manufacturer's instructions. Isolation of stable transfectants was performed as described earlier (12).

Immunostaining, Image Acquisition, and Processing—Immunofluorescence staining was carried out as described previously (19). Confocal images were acquired with a Zeiss LSM710 confocal microscope (Carl Zeiss) through a Plan-Apochromat ×63/1.40 NA oil-immersion objective lens (Carl Zeiss). Images were processed by Photoshop (Adobe). Projection of *Z*-stack images (0.3-μm sections) was acquired using Zen software (Carl Zeiss).

Small-angle X-ray Scattering Data Collection—Monomeric full-length αN-catenin samples at 10–78 μM in a storage buffer (25 mM Tris-HCl, pH 8.0, 150 mM NaCl, 1 mM TCEP) were used for SAXS data collection at McGill University and APS beamline 12. Both the monomeric and dimeric samples of αE-catenin were deemed unsuitable for SAXS analysis due to its heterogeneous nature. Home source data were measured on an Anton Paar SAXSess mc2 equipped with a PANalytical PW3830 x-ray generator and a Roper/Princeton CCD detector, with the sample temperature at 277 K. Synchrotron data were collected at the APS beamline 12-ID-C using the x-ray beam at 18 Kev and a MAR CCD detector, with the sample temperature at 277 K.

Small-angle X-ray Scattering Data Processing and Analysis—Data processing and analysis were performed using the ATSAS package (40); PRIMUS (41) was used for calculating the radius of gyration (R_g) and forward scattering (I_0) with the Guinier approximation; GNOM (42) was used to calculate the distance distribution function. The I_0 of each concentration was compared with lysozyme and bovine serum albumin datasets to verify the molecular weight and monomeric state, and to eliminate any potential for concentration-dependent effects. PRIMUS was used to produce a merged home source dataset for further analysis by combining a low-angle part of 15 μM data in the range of *S* from 0.002 to 0.089 nm^{-1} and a higher-angle part of 78 μM data in the range of *S* from 0.055 to 0.299 nm^{-1}. Similarly, a merged synchrotron dataset was produced for further analysis by combining a low-angle part of the 20 μM data in the range of S from 0.017 to 0.088 $Å^{-1}$ and a higher-angle part of 30 μM data in the range of *S* from 0.031 to 0.285 $Å^{-1}$. *Ab initio* shape reconstruction was carried out by generating 20 bead models with DAMMIN (43), and averaging with DAMAVER (44). Theoretical scattering curves were computed with CRYSOL (45). Rigid-body docking of the αEcatNM and αNcatC crystal structures into the SAXS-derived molecular envelope of αN-catenin was implemented using the six-dimensional search procedure in the Situs program package (46). Three-dimensional model of full-length αN-catenin was produced by using Modeller (47) with the docked crystal structures of αEcatNM and αNcatC, as well as full-length vinculin (PDB code 1ST6) as references, and used to calculate the theoretical scattering curve.

Pulldown Assays—GST-vinculin-D1 bound to glutathione resin (GE Healthcare) was incubated with αE-catenin samples (wild type, M371W, E521A, and R551A) or αN-catenin samples (wild type, M369W, E519A, and R549A) for 2 h at 277 K. Unbound αE- or αN-catenin samples were removed by gently washing the protein-bound resin with the binding buffer (20 mM Tris-HCl, pH 8.0, 100 mM NaCl, 1 mM TCEP). GST-vincu-

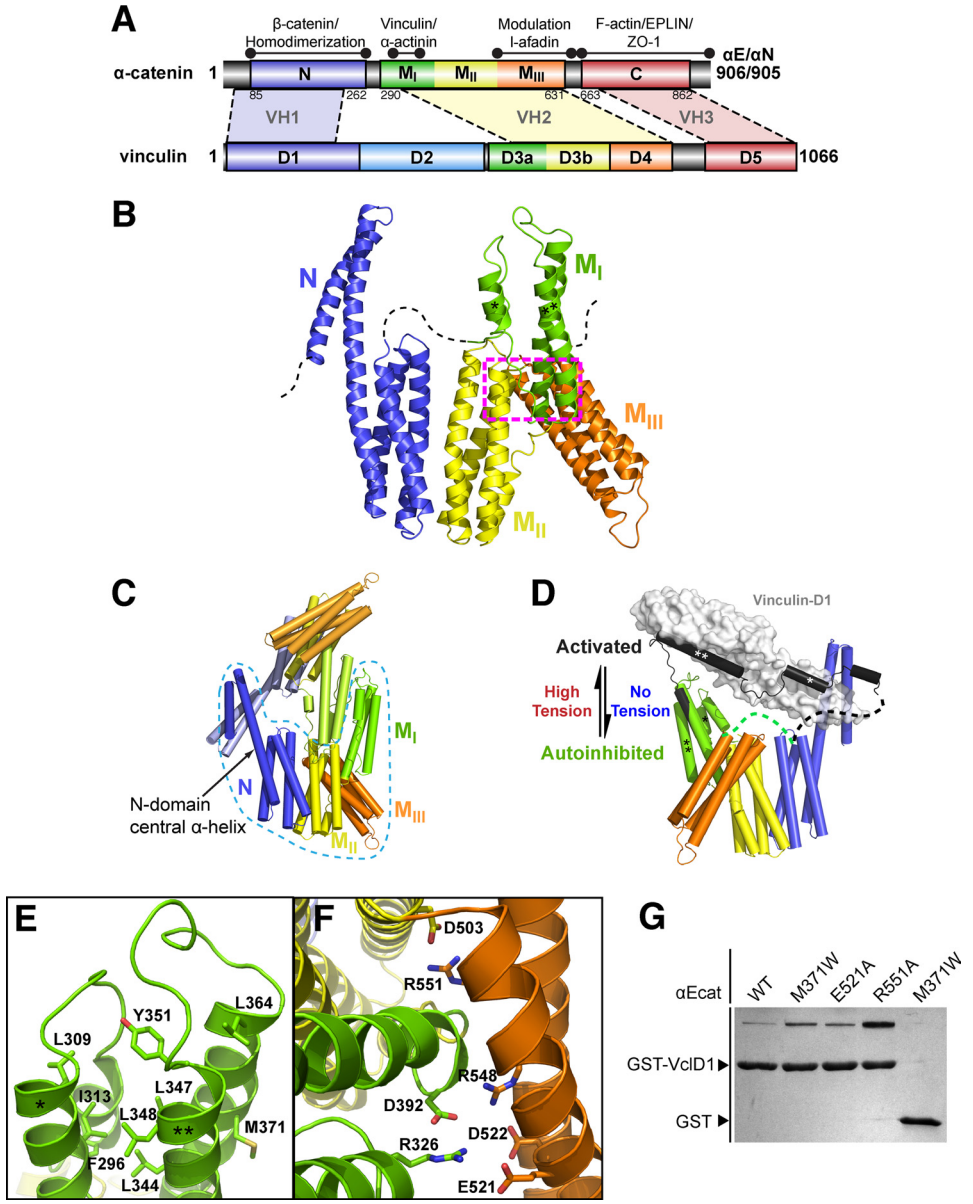

FIGURE 1. **Crystal structure of αEcatNM in the autoinhibited conformation.** *A,* α-catenin architecture. α-Catenin contains three major domains: N, M, and C. Structured regions are indicated by *colored boxes* with αE-catenin residue numbers shown *below*. Vinculin contains five domains, D1–D5. α-Catenin shares ~30% sequence identity with vinculin at Vinculin Homology regions, VH1, VH2, and VH3. *B,* 6.5-Å structure of αEcatNM. The VBS consists of the second and third α-helices (indicated by *single* and *double asterisks*, respectively) of the M_I bundle. *C,* homodimer structure of the αEcatNM. One protomer is outlined by a *cyan dashed line*. Two chains of αE-catenin form an asymmetric dimer with two juxtaposed M_I bundles. *D,* the unfurled structure of the M_I region bound to the D1 domain of vinculin (PDB code 4EHP; M_I in *black* and D1 in *gray*) (30) is aligned to the fourth helix of the M_I bundle (*green*) in the autoinhibited state. *E,* close-up view of the four-helix bundle formed by the M_I region. Amino acid residues in the hydrophobic core of the M_I bundle are shown as *sticks*. *F,* numerous salt bridges formed between charged residues (*sticks*) from different regions are involved in the stabilization of the M_I-M_{III} and M_{II}-M_{III} interfaces. The location of these interfaces is indicated by a *magenta box* in *B*. *G,* GST-vinculin-D1/GST pulldown assay with wild type αE-catenin or its single residue mutants, M371W, E521A, and R551A. The M371W mutant was designed to directly disrupt the M_I bundle (Fig. 1*E*).

lin-D1 and the bound protein samples were coeluted with 10 mM reduced glutathione.

Light Scattering—Multi-angle light scattering measurements were done in-line with size exclusion chromatography by using a three-angle (45°, 90°, and 135°) miniDawn light-scattering instrument and an Optilab rEX differential refractometer (Wyatt Technologies). Molecular weight was calculated by using the ASTRA software (Wyatt Technologies).

Actin-pelleting Assays—Monomeric rabbit skeletal muscle actin (Cytoskeleton) was polymerized in the polymerization buffer (5 mM Tris-HCl, pH 8.0, 50 mM KCl, 2 mM $MgCl_2$, 1 mM ATP, 0.2 mM $CaCl_2$, 0.5 mM DTT) for 1 h. Equal volumes of F-actin (8 μM) and 4–16 μM α-catenin sample were mixed in the binding buffer (20 mM Tris-HCl, pH 8.0, 50 mM KCl, 75 mM $NaCl_2$, 2 mM $MgCl_2$, 1 mM ATP, 0.2 mM $CaCl_2$, 0.5 mM DTT, 0.5 mM TCEP) for 1 h at 277 K. F-actin with bound protein samples were cosedimented by centrifugation at 100,000 × *g* for 20 min. Supernatant and pellet fractions were analyzed by SDS-PAGE with Coomassie Blue stain. Gel band intensity was measured by using ImageJ (48).

Analytical Ultracentrifugation—Sedimentation equilibrium experiments on αE- and αN-catenins were carried out at the

Ultracentrifugation Service Facility in the Department of Biochemistry at the University of Toronto. 6–21 μM α-Catenin protein in a buffer containing 50 mM Tris-HCl, pH 8.0, 300 mM NaCl, 10 mM β-mercaptoethanol, and 1 mM TCEP was spun at 7000, 8000, and 9000 rpm, at 4 °C, in an An-60 Ti rotor in a Beckman Optima XL-A analytical ultracentrifuge. Absorbance was recorded at 230 and 280 nm. Data analysis was performed using the Origin MicroCal XL-A/CL-I Data Analysis Software Package Version 4.0.

Fluorescence Resonance Energy Transfer Spectroscopy—Multiple rounds of PCR were performed to produce a chimeric αN-catenin construct with Cerulean (49) inserted between Pro^{633} and Glu^{634}. To generate αN-catenin FRET constructs, Venus (50) was inserted into the αN-catenin-Cerulean construct by introducing a HindIII site at various locations in the C domain of αN-catenin (between Arg^{650}-Ser^{651}, Gly^{803}-Gly^{804}, or Phe^{905}-STOP) by mutagenesis. Emission spectra of purified αN-catenin-FRET proteins were acquired with a Shimadzu RF-5301-PC spectrofluorophotometer. Cerulean and Venus emission spectra were collected at 1-nm intervals from 445 to 600 nm with excitation at 433 nm using slit widths of 3 nm for excitation and 5 nm for emission.

Electron Microscopy—αN-catenin protein samples were diluted to 0.5 μM with a buffer containing 20 mM Tris-HCl, pH 8.0, 100 mM NaCl, and 1 mM TCEP, and applied to continuous carbon film-coated copper/rhodium EM grids that were previously subjected to glow-discharge in air. After 2 min of incubation, the samples were washed with distilled water, stained with 0.75% uranyl formate, blotted, and allowed to air-dry. Images acquired with an FEI F20 electron microscope equipped with a field emission gun and operating at an accelerating voltage of 200 kV and a magnification of ×19,000 were recorded on TVIPS F114 CCD camera.

Blue Native Polyacrylamide Gel Electrophoresis—The oligomeric states of αE- and αN-catenin protein samples were examined by performing blue native polyacrylamide gel electrophoresis as previously described (51).

Sequence Alignment—Multiple sequence alignment of αE-catenin (accession NP_033948.1), αN-catenin (accession NP_663785.2), αT-catenin (accession NP_808280.2), and vinculin (accession Q64727) was performed by using COBALT (52) and Jalview (53). Structural alignment of αNcatC, αEcatC, and the vinculin D5 domain was performed by using LSQMAN (54) and Swiss-PdbViewer (55).

RESULTS

We have crystallized full-length αE-catenin and determined a 6.5-Å resolution structure by molecular replacement. The structure of αE-catenin (Fig. 1*B*), designated αEcatNM, consists of the N domain residues 85–262 in the homodimer state (Fig. 1*C*) and M domain residues 290–631 in an autoinhibited conformation, with no density observed for the C domain and the preceding linker region. The N domain structure consists of two helical bundles sharing a long central α-helix (Fig. 1*C*), and resembles previously determined N-terminal domain structures of αE-catenin and vinculin (24, 56) (supplemental Fig. 3*A*). In the crystal, this domain facilitates homodimerization through two N-terminal helices from each protomer forming

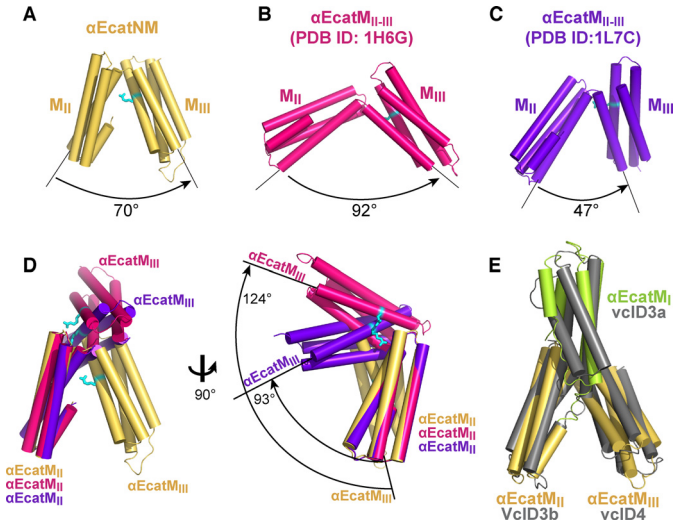

FIGURE 2. **Crystal structures of the αE-catenin M_{II-III} fragment.** *A*, crystal structure of the M_{II-III} fragment within αEcatNM. Angles between the M_{II} and M_{III} bundles are shown in *A–C*. *B*, crystal structure of the M_{II-III} fragment within the M fragment residues 377–633 (PDB code 1H6G) (25). *C*, crystal structure of the M_{II-III} fragment within the M fragment residues 385–651 (PDB code 1L7C) (28). The location of Arg^{551}, which is in close proximity with Asp^{503} to form salt bridges at the M_{II}-M_{III} interface in the αEcatNM structure (Fig. 1*F*), is shown as *cyan sticks*. *D*, previously determined structures of M_{II-III} fragments (PDB codes 1H6G and 1L7C) are superposed onto the M_{II-III} structure of αEcatNM by aligning the M_{II} bundles. The M_{III} bundles in PDB codes 1H6G and 1L7C are further rotated 124° and 93°, respectively, away from where the M_{III} bundle is located in αEcatNM, possibly due to the absence of N domain and M_{I} bundle. *E*, superposition of the M domain structure of αEcatNM and the D3–D4 domain structure of vinculin (PDB code 1ST6).

an intermolecular four-helix bundle in a similar manner as the previously described dimer domain structure (residues 82–279) (supplemental Fig. 3, *B* and *C*) (24). In addition, our αEcatNM structure reveals that the C-terminal four-helix bundle of the N domain is adjacently located to another bundle formed by the M_{II} region (residues 396–506) of the M domain (Fig. 1*B*). The M domain contains two additional four-helix bundles formed by M_{I} (residues 290–395) and M_{III} (residues 507–631) regions, and three bundles are organized into a "λ"-shaped configuration (Fig. 1*B*). The M_{I} region, which contains the vinculin-binding site (VBS; residues 305–352), forms a relatively short four-helix bundle consisting of two short and two long α-helices (Fig. 1*B*, supplemental Fig. S4, *A–D*), and this bundled conformation of M_{I} region is a stark contrast to the recently described unfurled or activated conformation of M_{I} region bound to the D1 domain of vinculin (29, 30) (Fig. 1*D*, supplemental Fig. S4*E*). Based on these crystallographic observations, we propose that the VBS adopts the "autoinhibited" conformation by occluding the vinculin-binding hydrophobic surfaces within the hydrophobic core of the M_{I} helical bundle (Fig. 1*E*). Unraveling of the helical bundle would allow the VBS to interact with vinculin through the "helix bundle conversion" mechanism (29, 30).

Previously, the M_{III} region was implicated in inhibiting the interaction between the VBS of α-catenin and vinculin (17). Our αEcatNM structure shows that the bundled conformation of the M_{I} region is supported by having its C terminus partially wedged between M_{II} and M_{III} bundles at the center of the M domain (Fig. 1*B*). Several charged amino acid residues from all three regions gather at the M_{I}-M_{III} and M_{II}-M_{III} interfaces to

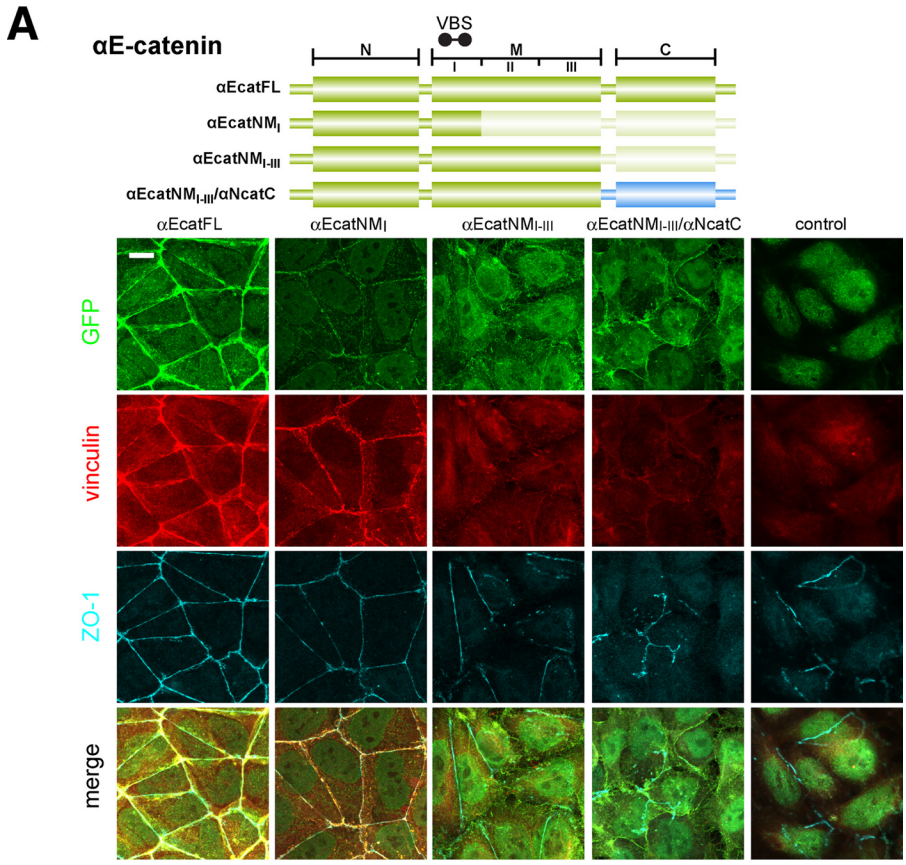
A
αE-catenin
VBS
N
M
C
I
II
III
αEcatFL
αEcatNMI
αEcatNMI-III
αEcatNMI-III/αNcatC
αEcatFL
αEcatNMI
αEcatNMI-III
αEcatNMI-III/αNcatC
control
GFP
vinculin
ZO-1
merge

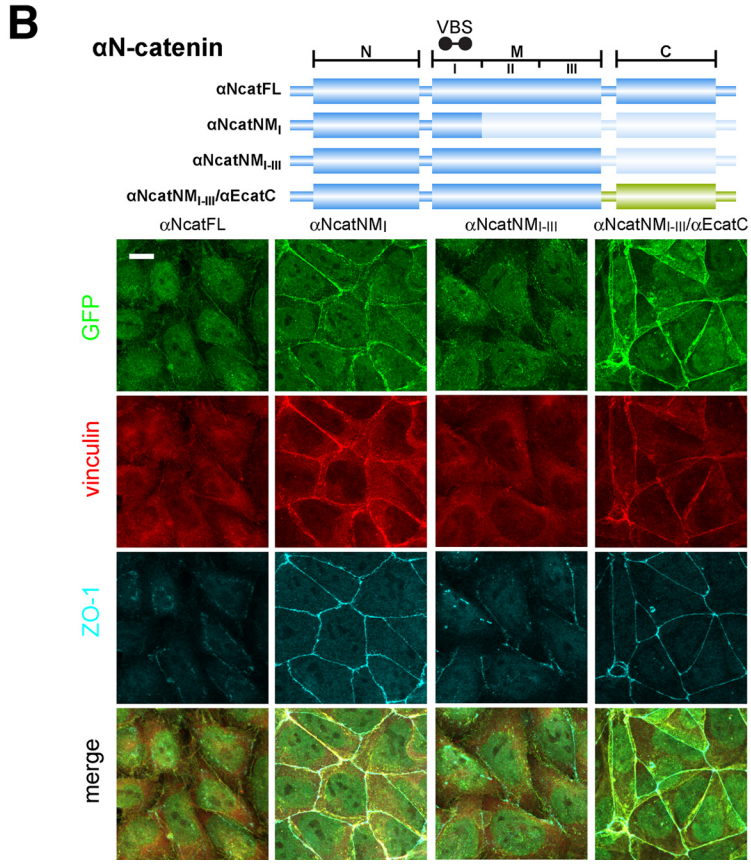
B
αN-catenin
VBS
N
M
C
I
II
III
αNcatFL
αNcatNMI
αNcatNMI-III
αNcatNMI-III/αEcatC
αNcatFL
αNcatNMI
αNcatNMI-III
αNcatNMI-III/αEcatC
GFP
vinculin
ZO-1
merge

form salt bridges (Fig. 1*F*). To examine how the conformational change of M_I region could be triggered by disrupting these inter-bundle interfaces, we made single-residue mutations within the M_{III} region of αE-catenin based on our structure and performed GST pulldown assays to test the ability of these variants to associate with vinculin. Comparing to the wild type αE-catenin, αE-catenin mutants R551A, and to lesser effect, E521A that are expected to disrupt the M_{II}-M_{III} and M_I-M_{III} interfaces (Fig. 1*F*), respectively, showed noticeable increases in binding to the D1 domain of vinculin (Fig. 1*G*). Similar observations were made with the equivalent mutations in αN-catenin (supplemental Fig. S5). Interestingly, the arrangement of the M_{II} and M_{III} bundles within αEcatNM is markedly different from previously determined M_{II-III} fragment structures in the absence of the N domain and the M_I region (Fig. 2, *A–D*) (25, 28), but surprisingly similar to the arrangement of D3–D4 domains in vinculin (Fig. 2*E*) (56, 57). This observation is particularly interesting as the compact arrangement of D3–D4 domains is stabilized through additional interdomain interactions involving the D2 domain, and the D3a bundle, which is equivalent to the M_I region of α-catenin, is less likely to "unfurl" due to the formation of a longer four-helix bundle (supplemental Fig. S4, *C* and *D*) (56). These structural features are missing in α-catenin (Fig. 1, *A* and *B*), which render α-catenin more conformationally "switchable" at the VBS. Together these observations suggest that the bundling of the M_I region effectively precludes vinculin from accessing the VBS and that the activation of VBS through unfurling of the M_I bundle is coupled to the destabilization of the compact arrangement of three helical bundles within the M domain.

We next asked how the autoinhibition could be released in cells and how multiple domains of αE- and αN-catenins contribute to the vinculin binding mechanism (17). We monitored the AJC formation and localization of vinculin by expressing α-catenin in the colon carcinoma-derived R2/7 cells, which are unable to organize the AJC due to the absence of α-catenin (26). We confirmed that typical AJC linearly delineating apical cell-cell boundaries are restored by expressing either full-length αE-catenin, which contains the C domain necessary to activate the autoinhibited VBS (17), or the NM_I fragment, which contains the VBS without the inhibitory M_{III} region, as monitored by co-immunostaining for ZO-1 (a tight junction protein), EGFP-tagged αE-catenin constructs and vinculin (Fig. 3*A*). In contrast, expression of the NM_{I-III} fragment of αE-catenin in R2/7 cells resulted in no typical AJC formation (Fig. 3*A*). In these cells, NM_{I-III} fragments containing the intact β-catenin binding site were only irregularly localized to cell-cell boundaries, where vinculin accumulation was less clear. Similar results are obtained when C-terminal truncation mutants of αN-catenin are expressed in R2/7 cells (Fig. 3*B*). However, R2/7 cells expressing full-length αN-catenin failed to establish the AJC, although faint vinculin signals were occasionally detectable together with this molecule, indicating that this "neural" α-catenin cannot normally function in this carcinoma line. Nevertheless, AJC formation, including vinculin recruitment to cell-cell boundaries, was induced in R2/7 cells expressing an αN/αE-chimera consisting of the αN-catenin NM domains fused with the αE-catenin C domain (Fig. 3*B*), but not with an αE/αN-chimera consisting of the αE-catenin NM domains fused with the αN-catenin C domain (Fig. 3*A*). Our *in vitro* actin-pelleting assay revealed that a significantly larger proportion of αE-catenin C domain (20 ± 2.7%) cosediments with F-actin compared with the αN-catenin C domain (12 ± 2.0%) (Fig. 4, *A* and *B*). These results support that the direct interaction between the α-catenin C domain and F-actin is critical for localization of vinculin at the AJC (17), and further suggest that the threshold of activation of α-catenin VBS is different in αE- and αN-catenins, with the C domain of αE-catenin having higher affinity for F-actin than the C domain of αN-catenin.

To examine the structural details responsible for direct F-actin interaction by α-catenin, we solved a crystal structure of the αN-catenin C domain (αNcatC), which consists of proteolytically stable residues 651–905 (supplemental Fig. S6), at 2.6-Å resolution (Fig. 4*C*). The αNcatC structure contains a five-helix bundle that closely resembles the actin-binding D5 domain structure of vinculin (58) (supplemental Fig. S7*A*). It has an additional α-helix preceding the bundle that caps the C-terminal end of the third α-helix, as well as the N-terminal (residues 651–661) and C-terminal extensions (residues 862–905) that are mostly disordered (Fig. 4*C*). Structural alignment of the actin-binding domains of αN-catenin and vinculin reveals that these structures are quite similar (root mean square deviation of 1.4 Å over 134 Cα atoms), but the residues proposed to be involved in the "upper" and "lower" F-actin-binding sites of vinculin are not well conserved in αN-catenin (59) (Fig. 4, *D–F*, supplemental Fig. S7, *B* and *C*). We then examined the electrostatic surface potential of αNcatC, which revealed prominent basic and acidic clusters similar to those located within the actin-binding domain of vinculin (supplemental Fig. S7, *D* and *E*). To gain insights into the differences in the actin-binding mechanisms of αN- and αE-catenins, we built a homology model of the αE-catenin C domain (αEcatC; residues 663–862) (supplemental Fig. S7*F*). As expected from the highly conserved primary sequences of αE and αN-catenins (supplemental Fig. S2), the structure and electrostatic surface potential of αEcatC resemble those of αNcatC (supplemental Fig. S7, *F* and *G*). However, careful inspection of the αE-catenin model identified an increased number of hydrophobic residues within the loop region (residues 849–856) following the α-helix 6 (Fig. 4, *D–F*). The location of this unique hydrophobic patch in the αEcatC model coincides with the lower actin-binding site of vinculin (59), suggesting a potential role in the enhanced association of αEcatC to F-actin.

FIGURE 3. **Junctional organization in R2/7 cells stably transfected with various αE-catenin (*A*) or αN-catenin (*B*) mutants tagged with EGFP, or transfected with EGFP only as a control.** Schematic figures represent a series of mutant constructs used. Cells were triple-immunostained for GFP, vinculin, and ZO-1 (a tight junction protein). αEcatFL, full-length αE-catenin; $\alpha EcatNM_I$, αE-catenin-NM_I fragment; $\alpha EcatNM_{I-III}$, αE-catenin-NM_{I-III} fragment; and $\alpha EcatNM_{I-III}$/αNcatC, a chimera consisting of αE-catenin-NM_{I-III} fragment fused to αN-catenin-C fragment. αNcatFL, full-length αN-catenin; $\alpha NcatNM_I$, αN-catenin-NM_I fragment; $\alpha NcatNM_{I-III}$, αN-catenin-NM_{I-III} fragment; and αNcat NM_{I-III}/αEcatC, a chimera consisting of αN-catenin-NM_{I-III} fragment fused to the αE-catenin-C fragment. *Scale bars*, 10 μm.

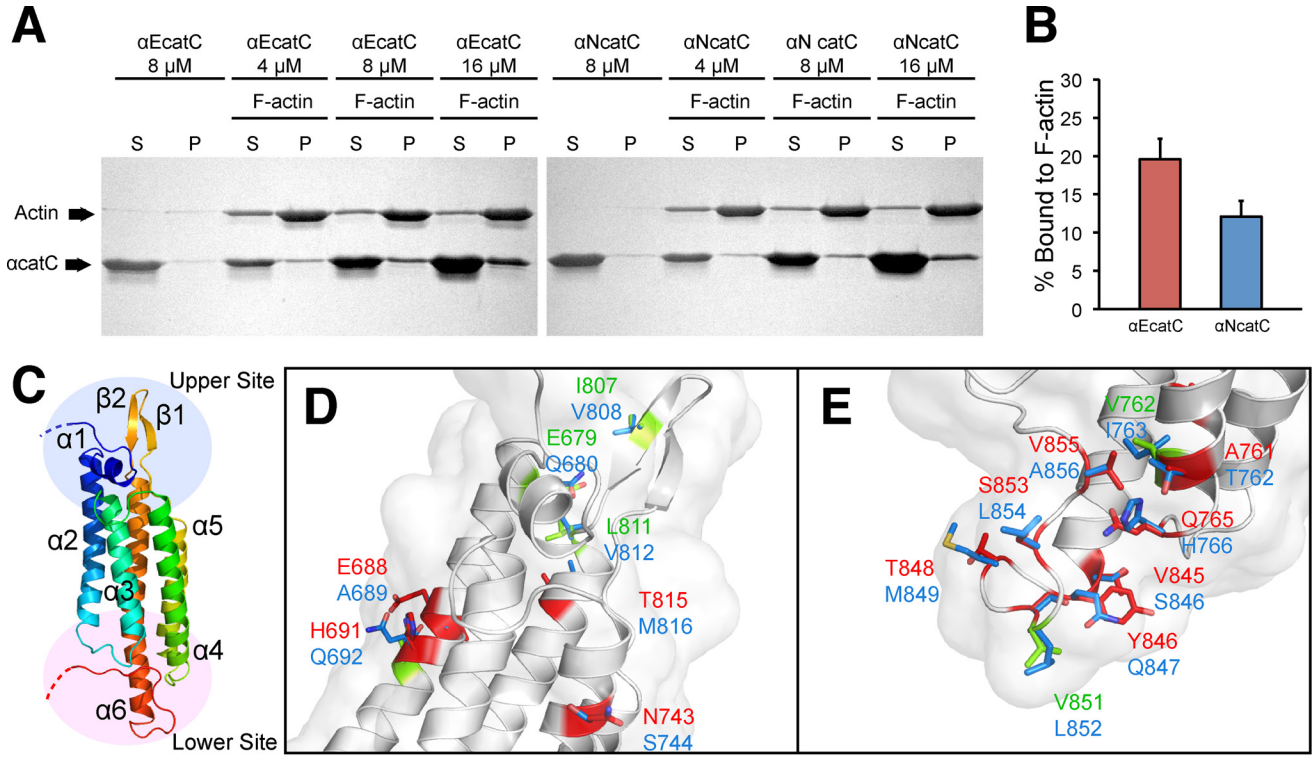

F

```
                 ---------- α1 ---------- α2 ----------
αNcat  651  srtsvqteddqLIAGQSARAIMAQLPQEEKAKIAEQVEIFHQEKSKLDAEVAKWDDSGND  710
αEcat  652  ..............................Q........AS.QE.........S........  711
Vcl    875                  PPPPEEKDEEFP.Q..GE.INQPMMM-AARQ.HD.AR..SSK...  918

                 ---------- α3 ---------- α4 ----------
αNcat  711  IIVLAKQMCMIMMEMTDFTRGKGPLKNTSDVINAAKKIAEAGSRMDKLARAVADQCPDSA  770
αEcat  712  ..........................................S..............G.TI..H.....  771
Vcl    919  ..AA..R.ALL.A..SRLV..G-SGNKR-AL.QC..D..K.SDEVTR..KE..KQ.T.KR  976

                 ---------- α5 ---------- β1 ---- β2 ---------- α6 ----------
αNcat  771  CKQDLLAYLQRIALYCHQLNICSKVKAEVQNLGGELIVSGLDSATSLIQAAKNLMNAVVL  830
αEcat  772  ..........................................V...V...M.............Q  831
Vcl    977  IRTN..QVCE..PTIST..K.L.T...TMLGRTNISDEESEQATEM.VHN.Q...QS.KE 1036

                 ----------------------------------------
αNcat  831  TVKASYVASTKYQKVYGTAAVNSPVVSWKMKapekkplvkrekpeefqtrvrrgsqkkhi  890
αEcat  832  ..............SQ.M.SL.L.A.................qd.t..kik.a.....v  891
Vcl   1037  ..REAEA..I.IRTD------AGFTLR.VR.TPWYQ                        1066

                 ------------
αNcat  891  spvqalsefkamdsf  905
αEcat  892  n............i  906
Vcl
```

FIGURE 4. **Crystal structure of the C domain of αN-catenin.** *A*, actin pelleting assays with αE-catenin C domain (αEcatC) and αN-catenin C domain (αNcatC). Supernatant (*S*) and pellet (*P*) fractions are indicated. *B*, the average percentage (and S.D.) of total protein cosedimenting with F-actin in three independent experiments was: αEcatC, 20.0(±2.6)%; αNcatC, 12.0(±2.0)%. *C*, crystal structure of αNcatC consists of six α-helices and a short β-hairpin and forms a five-helix bundle. Disordered N and C termini extensions are indicated by *dashed lines*. Regions equivalent to upper and lower actin-binding sites of vinculin (59)(supplemental Fig. S7*B*) are indicated. *D* and *E*, close-up views of the "upper site" (*D*) and "lower site" (*E*) of αN-catenin. Side chains of non-identical residues between αE-catenin (*blue*) and αN-catenin (*green* for conserved residues and *red* for non-conserved residues) are shown as sticks. *F*, structural alignment of actin-binding domain sequences of αN-catenin, αE-catenin, and vinculin (PDB code 1ST6). αE- and αN-catenins share 87% identical and 93% similar residues within their C domain sequences. αE-catenin and vinculin residues that are identical to αN-catenin residues are indicated by *dots*. Non-identical residues of αE-catenin are shown in *blue*, whereas αN-catenin residues in *green* and *red* indicate conserved and non-conserved substitutions found between αE- and αN-catenins. Vinculin residues that constitute the upper and lower sites (59) are shown as *orange* and *magenta*, respectively. Secondary structure information (*green bar* for α-helix and *red arrow* for β-strand) based on the crystal structures of αNcatC is shown.

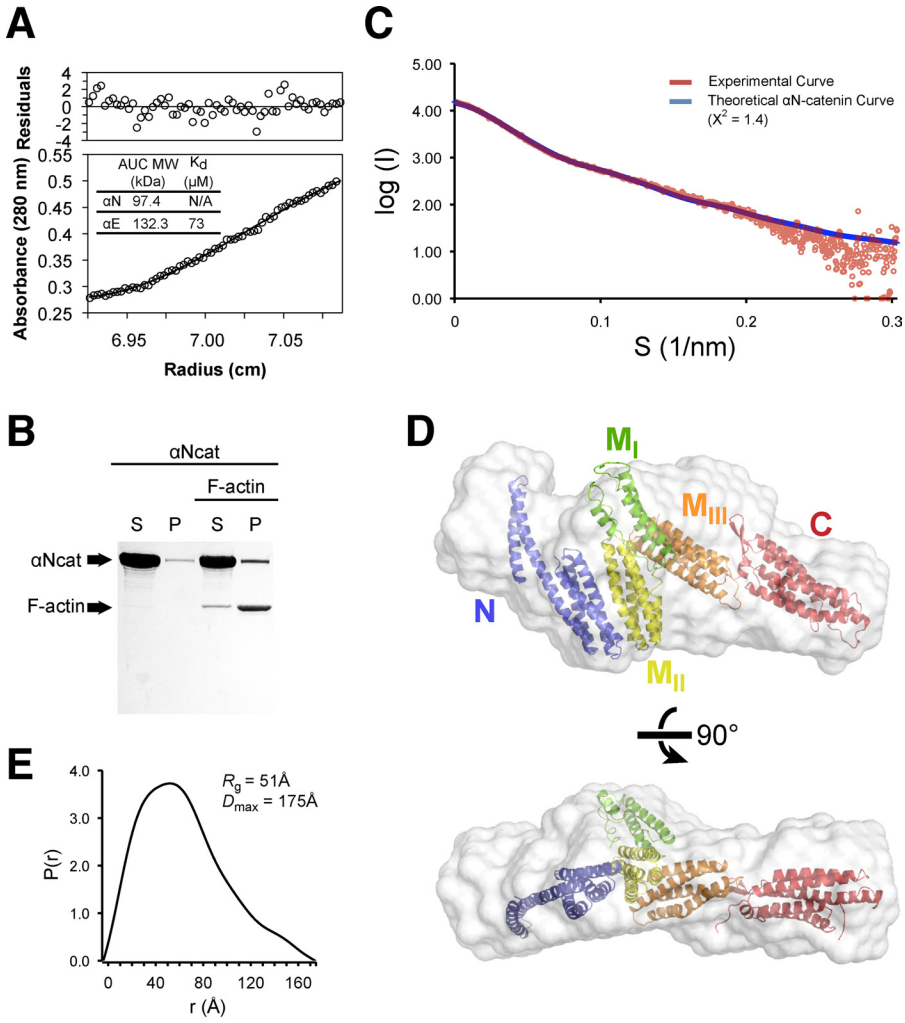

F

Protein	R_g (Å)	D_{max} (Å)	Reference
αN-catenin	51	175	this study
αNcatNM	46	154	this study
β-αE-catenin	45	150	(60)
αE-catenin dimer	60	193	(60)
HMP-1	37	123	(60)
Vinculin	37	121	(60)
*Dd*α-catenin	33	N/A	(61)

FIGURE 5. **Full-length structure of αN-catenin.** *A*, sedimentation equilibrium analysis of αN-catenin. αN-catenin exists as a monodisperse species with an average molecular mass of 97.4 kDa, which is approximately the size expected of a monomer. In contrast, αE-catenin exists in a monomer-dimer equilibrium (K_d = 73 μM) with an average molecular mass of 132.3 kDa. *B*, actin pelleting assay with full-length αN-catenin (αNcat). *C*, experimental scattering curve (*red*) of αN-catenin and a fitted theoretical scattering curve (*blue*) (χ^2 = 1.4) of its full-length structure model (supplemental Fig. S9*A*). *D*, docked crystal structures of αEcatNM and αNcatC within the *ab initio* molecular envelope of full-length αN-catenin (*gray*). *E*, pairwise distance-distribution function of αN-catenin scattering data. *F*, comparison of the R_g and D_{max} values obtained for αN-catenin to values previously reported for other α-catenins and vinculin (60, 61).

To gain further insights into how functionally distinct N, M, and C domains are physically coupled together in α-catenin, we performed the SAXS analysis of full-length αN-catenin. We determined that αN-catenin is suitable for the SAXS analysis, as analytical ultracentrifugation (Fig. 5*A*), size exclusion chromatography with multi-angle light scattering (supplemental Fig. S8*A*), blue native polyacrylamide gel electrophoresis (BN-PAGE) (supplemental Fig. S8*B*), and electron microscopy (supplemental Fig. S8*C*) confirmed that it predominantly exists as a monomer in solution (20). In contrast, αE-catenin exists as both monomer and dimer *in vitro* (14, 20). We also show that our recombinant full-length αN-catenin protein is functionally active, as it binds to F-actin in its monomeric state (Fig. 5*B*). Based on the scattering curve (Fig. 5*C*), the *ab initio* molecular envelope of full-length αN-catenin was calculated (Fig. 5*D*). It has an elongated shape that reflects the empirically determined radius of gyration (R_g) of 51 Å and maximum dimension (D_{max}) of 175 Å (Fig. 5*E*). Computational docking of αEcatNM and αNcatC crystal structures into the molecular envelope of αN-catenin revealed that the C domain is located near the M_{III}

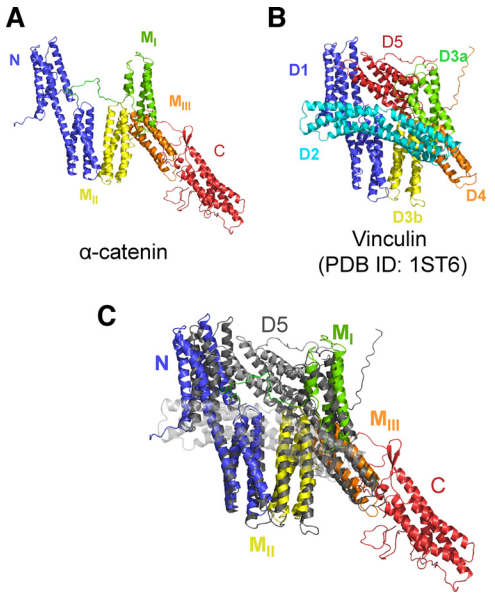

FIGURE 6. **Comparison of the multidomain structures of vinculin and αN-catenin.** Three individual domains (N, M, and C) of α-catenin share high structural homology with their equivalent domains of vinculin (D1, D3–D4, and D5) (supplemental Fig. S3*A*, S2*E*, and S7*A*). *A*, the elongated structure of full-length αN-catenin. *B*, the full-length crystal structure of vinculin (PDB code 1ST6) in the globular state. The actin-binding D5 domain forms interdomain interactions with the vinculin head region consisting of D1–D4 domains in a "pincer-shape" (56). *C*, superposition of αN-catenin and vinculin (*gray*). The D2 domain of vinculin is shown as a *transparent ribbon* to help visualize other structural features. The spatial arrangements of the N and M domains of α-catenin highly resemble the "pincer"-shaped arrangement of D1, D3, and D4 domains required for clamping the D5 domain and partially occluding the actin-binding sites (56).

bundle of the NM domains (Fig. 5*D*). The relative location of the C domain is further supported by a good agreement of our full-length αN-catenin model (supplemental Fig. S9*A*) with the experimental scattering curves (Fig. 5*C*, supplemental Fig. S9*B*) and the shorter D_{max} (154 Å) (Fig. 5*F*) of the αN-catenin mutant devoid of the C domain (αNcatNM), which yielded a truncated molecular envelope (supplemental Fig. S9*C*). The orientation of the docked C domain relative to the NM domains in the full-length model is consistent with our fluorescence resonance energy transfer (FRET) studies (supplemental Fig. S9, *D–F*), which indicated that the β-hairpin motif of the C domain is in close proximity to the C terminus of the M domain. These observations confirm that αN-catenin predominantly exists as a monomer with the elongated conformation that exposes a large portion of the actin-binding C domain (Fig. 5*D*). This structural feature is also consistent with full-length αN-catenin binding to F-actin during *in vitro* co-sedimentation assays (Fig. 5*B*). Comparison of the SAXS profile of αN-catenin with previously reported R_g and D_{max} values of related molecules (Fig. 5*F*) (60, 61) suggests that the monomeric β-αE-catenin chimera likely adopts an elongated conformation similar to αN-catenin, whereas HMP-1, an α-catenin homolog from *Caenorhabditis elegans*, is more likely to resemble the globular conformation of vinculin (56, 57). Superposition of our full-length αN-catenin model and a crystal structure of full-length vinculin (PDB code 1ST6) reveal that the assembly of N and M domains of αE-catenin is remarkably similar to the pincer-shaped arrangement of D1–D4 domains in vinculin (Fig. 6, *A* and *B*), however, unlike the D5 domain in vinculin, the C domain does not fold back toward the N terminus (Fig. 6*C*). Taken together, we propose that αE- and αN-catenin monomers in solution exist in the elongated conformation comprising the autoinhibited VBS with the C domain unhindered for F-actin interaction.

DISCUSSION

In this study, we have determined the three-dimensional structure of full-length α-catenin in the autoinhibited state, revealing its unique multidomain assembly necessary for α-catenin to act as a mechanosensor at AJs. The elongated structure of α-catenin consists of the centrally located, conformationally switchable modulatory domain flanked by the N-terminal β-catenin-binding domain and the C-terminal actin-binding domain. This domain arrangement and the fully accessible key ligand-binding sites on both N and C termini appear to be crucial for mechanically coupling the individual domain functionality to the conformational states of α-catenin. Moreover, it differentiates α-catenin from vinculin, which likely evolved from a common ancestral actin-binding protein involved in cell polarity of unicellular organisms (61).

Recently, the dimer structure of human αE-catenin mutant lacking the first 81 residues (ΔN-αE-catenin) was determined (62). It revealed that the N and M domains are similarly arranged as the mouse αEcatNM structure (Fig. 1*B*), but the relative location of the C domain differs from where this domain is positioned in our full-length mouse αN-catenin model. Interestingly, the C domain of ΔN-αE-catenin is folded back toward the M domain, but the relative orientation of C domains of the two protomers in the ΔN-αE-catenin dimer differs by almost 180° (62). Furthermore, the D_{max} of the human ΔN-αE-catenin crystal dimer (~130 Å) and the protomers in the dimer (~105 Å) are considerably shorter than previously reported D_{max} values of mouse αE-catenin dimer and monomer in solution (Fig. 5*F*) (60). We believe that variations of the C domain location among our αN-catenin model and the two protomers of the human ΔN-αE-catenin dimer may have resulted from the highly mobile nature of the C domain in both solution and crystal. In the crystallographic studies of human ΔN-αE-catenin (62), a crystal dehydration procedure employed to improve the crystal diffraction quality may have contributed to the observation of the compact conformation and domain rearrangements (63). In essence, these results together strongly suggest that the C domain of α-catenin is relatively mobile and not likely to adopt a fixed conformation within a full-length molecule in solution.

In our proposed model (Fig. 7*A*), unique "open" and "closed" conformations of α-catenin at AJs allow this molecule to couple the activation of autoinhibited VBS to the tension-sensitive actin-bound state of the C domain described previously (17). This "switch"-like mechanism provides the adjustable connectivity between cell junctions and the actin cytoskeleton necessary to counterbalance the actomyosin-generated tension by recruiting additional actin-binding protein vinculin to cell junctions (Fig. 3) (17). In the no-tension state, autoinhibited α-catenin forms a "closed (off)" conformation with the C domain of α-catenin capable of directly interacting with F-ac-

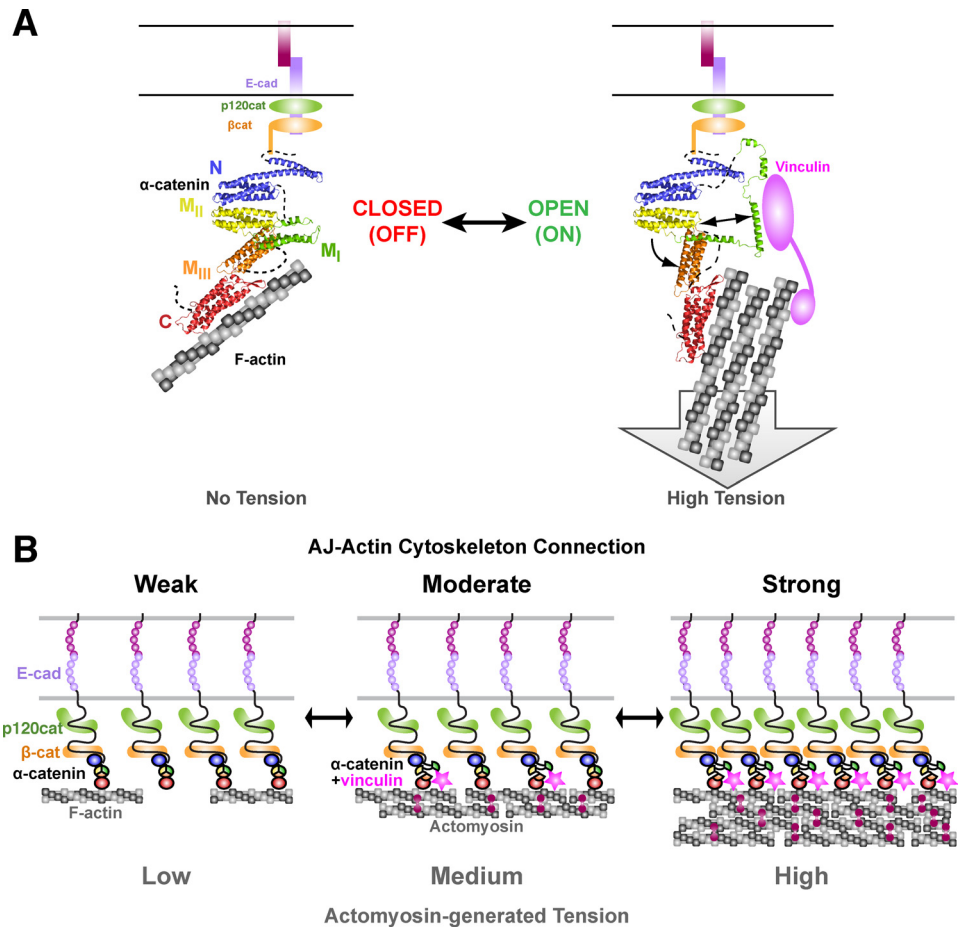

FIGURE 7. **Model for α-catenin-mediated localization of vinculin at AJs.** *A*, model of tension-dependent activation of α-catenin involving multistate conformational changes. α-Catenin acts as a "molecular switch" to modulate the connection between the cadherin-catenin complex and the actin cytoskeleton. In the no-tension state, the VBS within the M_I region remains closed (*OFF*) as there is no force being sensed by the C domain. In the high-tension state, the actomyosin-generated contractile force is detected by the C domain and helps to trigger "open to closed" conformational changes (*black arrows*) within the M domain. The VBS in the open (*ON*) conformation allows the activated vinculin to localize with the cadherin-catenin complex and engage in F-actin binding. *B*, model of the tension-dependent AJ-actin cytoskeleton connections regulated by cadherin-catenin-vinculin complexes.

tin, but the VBS remains in the bundled conformation (Fig. 7*A*). In the high-tension state, α-catenin adopts the "open (on)" conformation as the contraction of actomyosin filaments "pulls" the actin-bound C domain and triggers multistate conformational changes of the M domain, involving unclasping of the M_I bundle by the inhibitory M_{III} region and the subsequent "unfurling" of the VBS (Fig. 7*A*). As the activated pool of vinculin is expected to interact with the VBS of α-catenin (29, 30), it is likely that vinculin localized at AJs also engages in actin binding, hence further reinforcing the connectivity between the cadherin-catenin complex and the F-actin. The strength of anchoring the AJ to the actin cytoskeleton can be dynamically regulated to match the actomyosin-generated tension by adjusting the polarized distribution of the cadherin-catenin complex (64), as well as the number of activated α-catenins and vinculins at AJs (Fig. 7*B*). On the other hand, the dissipation of contractile forces would favor the α-catenin-vinculin interaction to dissociate and return α-catenin into the no-tension state signified by the "closed" conformation (Fig. 7*B*). In epithelia, the C domain of αE-catenin could directly bind to F-actin and/or indirectly through EPLIN to further stabilize the actin belts at zonula adherens (12). The relatively limited capacity of the C domain of αN-catenin to activate the VBS in R2/7 cells suggests that neuronal cells, the major cell types requiring αN-catenin (65) for their interactions, could express other regulators for the conformational changes of this catenin, which are missing in this carcinoma line.

Collectively, the present study provides the first *bona fide* structure of the autoinhibited state of α-catenin for its vinculin-binding activity, which is critical for the tension-dependent regulation of the linkages between the cadherin-catenin complex and the actin cytoskeleton. Unlike the globular structure of vinculin, the elongated conformation of α-catenin in an autoinhibited state suggests that α-catenins at AJs could associate with F-actin, but requires actomyosin-generated mechanical force (17) to trigger the conformational changes within the M domain and activate its vinculin-binding activity. Varied tension sensitivity of α-catenin and conformational dynamics displayed by different α-catenin isoforms and homologs are likely tailored to their tissue-/organism-specific functions, and could be further adjusted by other binding partners and post-translational modifications. The multidomain assembly of α-catenin revealed in this study is crucial for further delineating how α-catenin serves as a focal point to integrate various signals into regulating the stability of the AJs.

Acknowledgments—We are grateful to P. L. Howell, Y. Lobsanov, R. Julien, and A. Dong for assistance with crystal screening. We are grateful to the staff of the Advanced Photon Source (APS) beamline 19 for help with protein crystallography data collection. We thank X. Fang, S. Seifert, R. Winans, and Y. Wang at APS beamline 12 for assistance with SAXS data collection. We thank J. Dawson and A. Loncar for help with the actin-pelleting assay. We thank Y. Kakihara for assistance with analytical ultracentrifugation data collection and analysis. We thank A. Nagafuchi for providing the αE-catenin cDNA.

REFERENCES

1. Meng, W., and Takeichi, M. (2009) Adherens junction. Molecular architecture and regulation. *Cold Spring Harbor Perspect. Biol.* **1,** a002899
2. Tamada, M., Perez, T. D., Nelson, W. J., and Sheetz, M. P. (2007) Two distinct modes of myosin assembly and dynamics during epithelial wound closure. *J. Cell Biol.* **176,** 27–33
3. Vasioukhin, V., and Fuchs, E. (2001) Actin dynamics and cell-cell adhesion in epithelia. *Curr. Opin. Cell Biol.* **13,** 76–84
4. Takeichi, M. (1995) Morphogenetic roles of classic cadherins. *Curr. Opin. Cell Biol.* **7,** 619–627
5. Ishiyama, N., Lee, S.-H., Liu, S., Li, G.-Y., Smith, M. J., Reichardt, L. F., and Ikura, M. (2010) Dynamic and static interactions between p120 catenin and E-cadherin regulate the stability of cell-cell adhesion. *Cell* **141,** 117–128
6. Kobielak, A., and Fuchs, E. (2004) α-Catenin. At the junction of intercellular adhesion and actin dynamics. *Nat. Rev. Mol. Cell Biol.* **5,** 614–625
7. Ding, L., Ellis, M. J., Li, S., Larson, D. E., Chen, K., Wallis, J. W., Harris, C. C., McLellan, M. D., Fulton, R. S., Fulton, L. L., Abbott, R. M., Hoog, J., Dooling, D. J., Koboldt, D. C., Schmidt, H., Kalicki, J., Zhang, Q., Chen, L., Lin, L., Wendl, M. C., McMichael, J. F., Magrini, V. J., Cook, L., McGrath, S. D., Vickery, T. L., Appelbaum, E., Deschryver, K., Davies, S., Guintoli, T., Lin, L., Crowder, R., Tao, Y., Snider, J. E., Smith, S. M., Dukes, A. F., Sanderson, G. E., Pohl, C. S., Delehaunty, K. D., Fronick, C. C., Pape, K. A., Reed, J. S., Robinson, J. S., Hodges, J. S., Schierding, W., Dees, N. D., Shen, D., Locke, D. P., Wiechert, M. E., Eldred, J. M., Peck, J. B., Oberkfell, B. J., Lolofie, J. T., Du, F., Hawkins, A. E., O'Laughlin, M. D., Bernard, K. E., Cunningham, M., Elliott, G., Mason, M. D., Thompson, D. M., Ivanovich, J. L., Goodfellow, P. J., Perou, C. M., Weinstock, G. M., Aft, R., Watson, M., Ley, T. J., Wilson, R. K., and Mardis, E. R. (2010) Genome remodelling in a basal-like breast cancer metastasis and xenograft. *Nature* **464,** 999–1005
8. Park, C., Falls, W., Finger, J. H., Longo-Guess, C. M., and Ackerman, S. L. (2002) Deletion in Catna2, encoding α N-catenin, causes cerebellar and hippocampal lamination defects and impaired startle modulation. *Nat. Genet.* **31,** 279–284
9. van Hengel, J., Calore, M., Bauce, B., Dazzo, E., Mazzotti, E., De Bortoli, M., Lorenzon, A., Li Mura, I. E. A., Beffagna, G., Rigato, I., Vleeschouwers, M., Tyberghein, K., Hulpiau, P., van Hamme, E., Zaglia, T., Corrado, D., Basso, C., Thiene, G., Daliento, L., Nava, A., van Roy, F., and Rampazzo, A. (2013) Mutations in the area composita protein αT-catenin are associated with arrhythmogenic right ventricular cardiomyopathy. *Eur. Heart J.* **34,** 201–210
10. Sarpal, R., Pellikka, M., Patel, R. R., Hui, F. Y., Godt, D., and Tepass, U. (2012) Mutational analysis supports a core role for *Drosophila* α-catenin in adherens junction function. *J. Cell Sci.* **125,** 233–245
11. Watabe, M., Nagafuchi, A., Tsukita, S., and Takeichi, M. (1994) Induction of polarized cell-cell association and retardation of growth by activation of the E-cadherin-catenin adhesion system in a dispersed carcinoma line. *J. Cell Biol.* **127,** 247–256
12. Taguchi, K., Ishiuchi, T., and Takeichi, M. (2011) Mechanosensitive EPLIN-dependent remodeling of adherens junctions regulates epithelial reshaping. *J. Cell Biol.* **194,** 643–656
13. Abe, K., Chisaka, O., Van Roy, F., and Takeichi, M. (2004) Stability of dendritic spines and synaptic contacts is controlled by αN-catenin. *Nat. Neurosci.* **7,** 357–363
14. Drees, F., Pokutta, S., Yamada, S., Nelson, W. J., and Weis, W. I. (2005) α-Catenin is a molecular switch that binds E-cadherin-β-catenin and regulates actin-filament assembly. *Cell* **123,** 903–915
15. Yamada, S., Pokutta, S., Drees, F., Weis, W. I., and Nelson, W. J. (2005) Deconstructing the cadherin-catenin-actin complex. *Cell* **123,** 889–901
16. Rimm, D. L., Koslov, E. R., Kebriaei, P., Cianci, C. D., and Morrow, J. S. (1995) α_1(E)-catenin is an actin-binding and -bundling protein mediating the attachment of F-actin to the membrane adhesion complex. *Proc. Natl. Acad. Sci. U.S.A.* **92,** 8813–8817
17. Yonemura, S., Wada, Y., Watanabe, T., Nagafuchi, A., and Shibata, M. (2010) α-Catenin as a tension transducer that induces adherens junction development. *Nat. Cell Biol.* **12,** 533–542
18. le Duc, Q., Shi, Q., Blonk, I., Sonnenberg, A., Wang, N., Leckband, D., and de Rooij, J. (2010) Vinculin potentiates E-cadherin mechanosensing and is recruited to actin-anchored sites within adherens junctions in a myosin II-dependent manner. *J. Cell Biol.* **189,** 1107–1115
19. Abe, K., and Takeichi, M. (2008) EPLIN mediates linkage of the cadherin-catenin complex to F-actin and stabilizes the circumferential actin belt. *Proc. Natl. Acad. Sci. U.S.A.* **105,** 13–19
20. Desai, R., Sarpal, R., Ishiyama, N., Pellikka, M., Ikura, M., and Tepass, U. (2013) Monomeric α-catenin links cadherin to the actin cytoskeleton. *Nat. Cell Biol.* **15,** 261–273
21. Smutny, M., Cox, H. L., Leerberg, J. M., Kovacs, E. M., Conti, M. A., Ferguson, C., Hamilton, N. A., Parton, R. G., Adelstein, R. S., and Yap, A. S. (2010) Myosin II isoforms identify distinct functional modules that support integrity of the epithelial zonula adherens. *Nat. Cell Biol.* **12,** 696–702
22. Borghi, N., Sorokina, M., Shcherbakova, O. G., Weis, W. I., Pruitt, B. L., Nelson, W. J., and Dunn, A. R. (2012) E-cadherin is under constitutive actomyosin-generated tension that is increased at cell-cell contacts upon externally applied stretch. *Proc. Natl. Acad. Sci. U.S.A.* **109,** 12568–12573
23. Aberle, H., Butz, S., Stappert, J., Weissig, H., Kemler, R., and Hoschuetzky, H. (1994) Assembly of the cadherin-catenin complex *in vitro* with recombinant proteins. *J. Cell Sci.* **107,** 3655–3663
24. Pokutta, S., and Weis, W. I. (2000) Structure of the dimerization and β-catenin-binding region of α-catenin. *Mol. Cell* **5,** 533–543
25. Yang, J., Dokurno, P., Tonks, N. K., and Barford, D. (2001) Crystal structure of the M-fragment of α-catenin. Implications for modulation of cell adhesion. *EMBO J.* **20,** 3645–3656
26. Watabe-Uchida, M., Uchida, N., Imamura, Y., Nagafuchi, A., Fujimoto, K., Uemura, T., Vermeulen, S., van Roy, F., Adamson, E. D., and Takeichi, M. (1998) α-Catenin-vinculin interaction functions to organize the apical junctional complex in epithelial cells. *J. Cell Biol.* **142,** 847–857
27. Itoh, M., Nagafuchi, A., Moroi, S., and Tsukita, S. (1997) Involvement of ZO-1 in cadherin-based cell adhesion through its direct binding to α-catenin and actin filaments. *J. Cell Biol.* **138,** 181–192
28. Pokutta, S., Drees, F., Takai, Y., Nelson, W. J., and Weis, W. I. (2002) Biochemical and structural definition of the L-afadin- and actin-binding sites of α-catenin. *J. Biol. Chem.* **277,** 18868–18874
29. Choi, H.-J., Pokutta, S., Cadwell, G. W., Bobkov, A. A., Bankston, L. A., Liddington, R. C., and Weis, W. I. (2012) αE-catenin is an autoinhibited molecule that coactivates vinculin. *Proc. Natl. Acad. Sci. U.S.A.* **109,** 8576–8581
30. Rangarajan, E. S., and Izard, T. (2012) The cytoskeletal protein α-catenin unfurls upon binding to vinculin. *J. Biol. Chem.* **287,** 18492–18499
31. Otwinowski, Z., and Minor, W. (1997) Processing of X-ray diffraction data collected in oscillation mode. *Methods Enzymol.* **276,** 307–326
32. McCoy, A. J., Grosse-Kunstleve, R. W., Adams, P. D., Winn, M. D., Storoni, L. C., and Read, R. J. (2007) Phaser crystallographic software. *J. Appl. Crystallogr.* **40,** 658–674
33. Brünger, A. T., Adams, P. D., Clore, G. M., DeLano, W. L., Gros, P., Grosse-Kunstleve, R. W., Jiang, J. S., Kuszewski, J., Nilges, M., Pannu, N. S., Read, R. J., Rice, L. M., Simonson, T., and Warren, G. L. (1998) Crystallography & NMR system. A new software suite for macromolecular structure determination. *Acta Crystallogr. D Biol. Crystallogr.* **54,** 905–921
34. Schröder, G. F., Levitt, M., and Brunger, A. T. (2010) Super-resolution biomolecular crystallography with low-resolution data. *Nature* **464,** 1218–1222
35. Brunger, A. T., Adams, P. D., Fromme, P., Fromme, R., Levitt, M., and Schröder, G. F. (2012) Improving the accuracy of macromolecular struc-

ture refinement at 7-Å resolution. *Structure* **20,** 957–966
36. Emsley, P., and Cowtan, K. (2004) Coot. Model-building tools for molecular graphics. *Acta Crystallogr. D Biol. Crystallogr.* **60,** 2126–2132
37. Adams, P. D., Afonine, P. V., Bunkóczi, G., Chen, V. B., Davis, I. W., Echols, N., Headd, J. J., Hung, L.-W., Kapral, G. J., Grosse-Kunstleve, R. W., McCoy, A. J., Moriarty, N. W., Oeffner, R., Read, R. J., Richardson, D. C., Richardson, J. S., Terwilliger, T. C., and Zwart, P. H. (2010) PHENIX. A comprehensive Python-based system for macromolecular structure solution. *Acta Crystallogr. D Biol. Crystallogr.* **66,** 213–221
38. Baker, N. A., Sept, D., Joseph, S., Holst, M. J., and McCammon, J. A. (2001) Electrostatics of nanosystems. Application to microtubules and the ribosome. *Proc. Natl. Acad. Sci. U.S.A.* **98,** 10037–10041
39. Ichii, T., and Takeichi, M. (2007) p120-catenin regulates microtubule dynamics and cell migration in a cadherin-independent manner. *Genes Cells* **12,** 827–839
40. Konarev, P. V., Petoukhov, M. V., Volkov, V. V., and Svergun, D. I. (2006) ATSAS 2.1, a program package for small-angle scattering data analysis. *J. Appl. Crystallogr.* **39,** 277–286
41. Konarev, P. V., Volkov, V. V., Sokolova, A. V., Koch, M. H. J., and Svergun, D. I. (2003) PRIMUS. A Windows PC-based system for small-angle scattering data analysis. *J. Appl. Crystallogr.* **36,** 1277–1282
42. Svergun, D. I. (1992) Determination of the regularization parameter in indirect-transform methods using perceptual criteria. *J. Appl. Crystallogr.* **25,** 495–503
43. Svergun, D. I. (1999) Restoring low resolution structure of biological macromolecules from solution scattering using simulated annealing. *Biophys. J.* **76,** 2879–2886
44. Volkov, V. V., and Svergun, D. I. (2003) Uniqueness of *ab initio* shape determination in small-angle scattering. *J. Appl. Crystallogr.* **36,** 860–864
45. Svergun, D. I., Barberato, C., and Koch, M. (1995) CRYSOL. A program to evaluate x-ray solution scattering of biological macromolecules from atomic coordinates. *J. Appl. Crystallogr.* **28,** 768–773
46. Wriggers, W., and Birmanns, S. (2001) Using Situs for flexible and rigid-body fitting of multiresolution single-molecule data. *J. Struct. Biol.* **133,** 193–202
47. Sali, A., and Blundell, T. L. (1993) Comparative protein modelling by satisfaction of spatial restraints. *J. Mol. Biol.* **234,** 779–815
48. Schneider, C. A., Rasband, W. S., and Eliceiri, K. W. (2012) NIH Image to ImageJ. 25 years of image analysis. *Nat. Methods* **9,** 671–675
49. Rizzo, M. A., Springer, G. H., Granada, B., and Piston, D. W. (2004) An improved cyan fluorescent protein variant useful for FRET. *Nat. Biotechnol.* **22,** 445–449
50. Nagai, T., Ibata, K., Park, E. S., Kubota, M., Mikoshiba, K., and Miyawaki, A. (2002) A variant of yellow fluorescent protein with fast and efficient maturation for cell-biological applications. *Nat. Biotechnol.* **20,** 87–90
51. Wittig, I., Braun, H.-P., and Schägger, H. (2006) Blue native PAGE. *Nat. Protoc.* **1,** 418–428
52. Papadopoulos, J. S., and Agarwala, R. (2007) COBALT. Constraint-based alignment tool for multiple protein sequences. *Bioinformatics* **23,** 1073–1079
53. Waterhouse, A. M., Procter, J. B., Martin, D. M., Clamp, M., and Barton, G. J. (2009) Jalview Version 2. A multiple sequence alignment editor and analysis workbench. *Bioinformatics* **25,** 1189–1191
54. Kleywegt, G. J. (1996) Use of non-crystallographic symmetry in protein structure refinement. *Acta Crystallogr. D Biol. Crystallogr.* **52,** 842–857
55. Guex, N., and Peitsch, M. C. (1997) SWISS-MODEL and the Swiss-PdbViewer. An environment for comparative protein modeling. *Electrophoresis* **18,** 2714–2723
56. Bakolitsa, C., Cohen, D. M., Bankston, L. A., Bobkov, A. A., Cadwell, G. W., Jennings, L., Critchley, D. R., Craig, S. W., and Liddington, R. C. (2004) Structural basis for vinculin activation at sites of cell adhesion. *Nature* **430,** 583–586
57. Borgon, R. A., Vonrhein, C., Bricogne, G., Bois, P. R., and Izard, T. (2004) Crystal structure of human vinculin. *Structure* **12,** 1189–1197
58. Bakolitsa, C., de Pereda, J. M., Bagshaw, C. R., Critchley, D. R., and Liddington, R. C. (1999) Crystal structure of the vinculin tail suggests a pathway for activation. *Cell* **99,** 603–613
59. Janssen, M. E., Kim, E., Liu, H., Fujimoto, L. M., Bobkov, A., Volkmann, N., and Hanein, D. (2006) Three-dimensional structure of vinculin bound to actin filaments. *Mol. Cell* **21,** 271–281
60. Kwiatkowski, A. V., Maiden, S. L., Pokutta, S., Choi, H.-J., Benjamin, J. M., Lynch, A. M., Nelson, W. J., Weis, W. I., and Hardin, J. (2010) *In vitro* and *in vivo* reconstitution of the cadherin-catenin-actin complex from *Caenorhabditis elegans*. *Proc. Natl. Acad. Sci. U.S.A.* **107,** 14591–14596
61. Dickinson, D. J., Nelson, W. J., and Weis, W. I. (2011) A polarized epithelium organized by β- and α-catenin predates cadherin and metazoan origins. *Science* **331,** 1336–1339
62. Rangarajan, E. S., and Izard, T. (2013) Dimer asymmetry defines α-catenin interactions. *Nat. Struct. Mol. Biol.* **20,** 188–193
63. Esnouf, R. M., Ren, J., Garman, E. F., Somers, D. O., Ross, C. K., Jones, E. Y., Stammers, D. K., and Stuart, D. I. (1998) Continuous and discontinuous changes in the unit cell of HIV-1 reverse transcriptase crystals on dehydration. *Acta Crystallogr. D Biol. Crystallogr.* **54,** 938–953
64. Rauzi, M., Lenne, P.-F., and Lecuit, T. (2010) Planar polarized actomyosin contractile flows control epithelial junction remodelling. *Nature* **468,** 1110–1114
65. Uemura, M., and Takeichi, M. (2006) αN-catenin deficiency causes defects in axon migration and nuclear organization in restricted regions of the mouse brain. *Dev. Dyn.* **235,** 2559–2566